

T_1 - and T_2 -spin relaxation time limitations of phosphorous donor electrons near crystalline silicon to silicon dioxide interface defects

S.-Y. Paik, S.-Y. Lee, W. J. Baker, D. R. McCamey,* and C. Boehme[†]

University of Utah, Department of Physics and Astronomy, 115 South 1400 East, Salt Lake City, Utah

(Dated: November 8, 2018)

A study of donor electron spins and spin-dependent electronic transitions involving phosphorous (^{31}P) atoms in proximity of the (111) oriented crystalline silicon (c-Si) to silicon dioxide (SiO_2) interface is presented for $[^{31}\text{P}] = 10^{15} \text{ cm}^{-3}$ and $[^{31}\text{P}] = 10^{16} \text{ cm}^{-3}$ at about liquid ^4He temperatures ($T = 5 \text{ K} - 15 \text{ K}$). Using pulsed electrically detected magnetic resonance (pEDMR), spin-dependent transitions between the ^{31}P donor state and two distinguishable interface states are observed, namely (i) P_b centers which can be identified by their characteristic anisotropy and (ii) a more isotropic center which is attributed to E' defects of the SiO_2 bulk close to the interface. Correlation measurements of the dynamics of spin-dependent recombination confirm that previously proposed transitions between ^{31}P and the interface defects take place. The influence of these electronic near-interface transitions on the ^{31}P donor spin coherence time T_2 as well as the donor spin-lattice relaxation time T_1 is then investigated by comparison of spin Hahn-echo decay measurements obtained from conventional bulk sensitive pulsed electron paramagnetic resonance and surface sensitive pEDMR, as well as surface sensitive electrically detected inversion recovery experiments. The measurements reveal that both T_2 and T_1 of ^{31}P donor electrons spins in proximity of energetically lower interface states at $T \leq 13 \text{ K}$ are reduced by several orders of magnitude.

PACS numbers: 71.55.Cn, 72.25.Rb, 73.20.Hb, 76.30.Da

Keywords: silicon, phosphorus, electrically detected magnetic resonance, donor, interface defects, spin phase coherence

I. INTRODUCTION

Due to their technological importance, the properties of phosphorous (^{31}P) donors in crystalline silicon have been investigated extensively for more than half a century. During this time, magnetic resonance based methods have revealed many aspects of the microscopic nature of ^{31}P as well as the electronic processes in which it is involved. Since the first mapping of a donor wavefunction using an electron nuclear double resonance technique¹, a large and diverse amount of information regarding the electronic and quantum mechanical properties of such systems has been reported². This wealth of information has contributed to the technological exploitation of silicon to the extent that it has become the most widely utilized semiconductor in the global electronics industry. However, even with all the information regarding silicon available to us, there are still questions regarding the ability to exploit the quantum mechanical nature (specifically spin) of dopants and charge carriers for technological applications such as spin transistors³ or quantum computers⁴, the latter of which are proposed to utilize electron or nuclear spins of phosphorus donors in silicon as quantum bits. While there has been significant experimental effort for the implementation of these and other concepts⁵, challenges remain in a number of different areas, the most pressing being the difficulty in detecting the spin of individual donors without reducing its quantum memory time (the coherence time, T_2)⁶. Nevertheless, donors in silicon retain promise in this area due to their extremely long phase coherence times, with T_2 exceeding 60 ms for the electron spin⁷ and 1 second for the nuclear spin⁸ at liquid He temperatures.

Many of the recent schemes for silicon based spin- or quan-

tum devices involve electronic processes occurring at or near interfaces, particularly the c-Si/ SiO_2 interface. This presents advantages since locating spins near interfaces allows them to be controlled with surface gates⁴, and detected with surface electronics^{9,10,11,12,13}. However, it may also lead to a decrease in spin coherence due to the spin-spin interactions with surface states^{14,15}, as well as to the loss of quantum information following spin-dependent recombination through surface states. Since it is not possible to obtain defect free c-Si/ SiO_2 interfaces¹⁶ (we note that work is currently being undertaken to obtain defect free interfaces using H-termination but it is in the very early stages^{17,18}) and since there are even proposals to use interface defects as probe spins to readout⁹ the spin of a single donor, the understanding of interface electron and spin transitions has become important.

In the following, pulsed electrically detected magnetic resonance (pEDMR) and pulsed electron paramagnetic resonance (pEPR) measurements performed on (111) surface oriented c-Si samples with $[\text{P}] = 10^{15} \text{ cm}^{-3}$ and $[\text{P}] = 10^{16} \text{ cm}^{-3}$ at temperatures between $T = 5 \text{ K}$ and $T = 15 \text{ K}$ are presented. The data was collected in order to elucidate the nature of spin-dependent electronic interface transitions involving ^{31}P donor and interface states and to then determine how these processes influence the coherence time of the ^{31}P donor electron spins in proximity of these interface defects. The latter was accomplished by comparison of the interface sensitive pEDMR measurements to bulk sensitive pEPR measurements of ^{31}P donors. Our results are discussed with regard to their implications for the ability of spin qubit readout using interface defect probe spins whilst maintaining long coherence times. We emphasized that while the key questions motivating this study are centered about ^{31}P qubit coherence times, the study presented follows an extensive number of previous EPR^{19,20,21,22,23,24,25},

EDMR^{10,25,26,27,28} and pEDMR^{29,30,31} studies carried out on various c-Si/SiO₂ interface defects as well as electronic trapping and recombination processes of interfaces with different surface orientations and ³¹P doping concentrations. Most of these studies aimed to enhance the understanding of electronic processes relevant for materials systems used in conventional c-Si based microelectronics and photovoltaic devices. Thus, the study presented here may also be of relevance for conventional silicon technologies.

II. EXPERIMENTS

Following the recent demonstration of electrical detection of ³¹P spin states¹⁰ we anticipate, for the pEDMR measurements presented here, the presence of spin-dependent recombination between ³¹P donor states and energetically lower c-Si/SiO₂ interface states, as illustrated for the example of the P_b interface state in Fig. 1. Figure 1(a) displays a geometrical stick and ball sketch of the c-Si/SiO₂ interface where some of the silicon (111) surface atoms possess unsaturated bonds (called dangling bonds). These dangling bonds are all oriented along the (111) axis²⁵ and are highly localized states with much p-content and only small s-content^{32,33}. Silicon dangling bonds oriented along the (111) direction (also called P_b centers) are highly anisotropic and, since they are paramagnetic when uncharged^{19,34}, can be identified using EPR by their well known Landé (g) factor anisotropy²⁵, revealed by measurement of EPR spectra as a function of the angle θ between the B_0 field and the (111) direction (see sketch). In contrast to the P_b state, the shallow ³¹P donor state (illustrated by the large shaded circle in Fig. 1(a)) is a significantly less localized state having an s-like envelope function with a localization length of ≈ 3 nm, strongly modulated by the periodic crystalline structure of its host environment^{35,36}. Since the ³¹P donor state encompasses thousands of silicon sites, an exchange interaction between near-surface ³¹P donors and P_b centers can occur allowing the transition of the donor electron into the energetically lower interface state. This transition is sketched for an interface band diagram in Fig. 1(b). The illustration shows that: (i) Both the ³¹P donor state as well as the P_b state become charged (positively and negatively, respectively) through the transition. (ii) Because of the Pauli principle, and spin conservation due to the weak spin-orbital coupling of silicon, the transition is spin-dependent. Hence, the transition provides a spin-to-charge conversion mechanism and as a result, since the charge of the ³¹P⁺/P_b⁻ can be detected through the measurement of recombination currents, ³¹P/P_b pairs have been proposed as electric readout mechanism for ³¹P qubits^{9,10}.

Experimentally, time domain measurements of spin-dependent c-Si/SiO₂ interface recombination were conducted in order to verify that the qualitative behavior of interface currents after EPR excitation of the ³¹P or the P_b states is similar to higher doped c-Si samples with (100) orientation. In order to also verify electrically detect spin-Rabi oscillation (as expected from previous studies^{6,10}), transient-nutation-like measurements of the integrated current transients as a

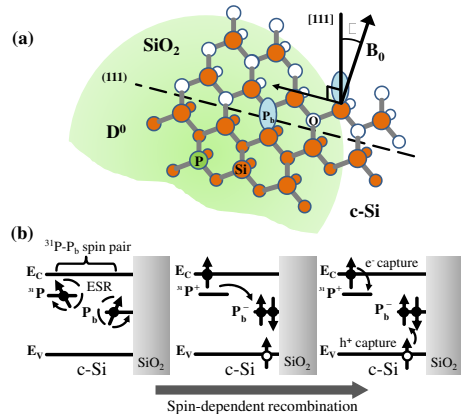


Figure 1: (color online) (a) Ball and stick illustration of the atom scale structure of the c-Si/SiO₂ interface. The ³¹P donor state (green circle) is significantly larger than the P_b center. Exchange coupling between the two states is possible when they are sufficiently close to each other. The orientation of the interface is defined by the angle θ between the externally applied B_0 magnetic field and the (111) crystal axis which is perpendicular to the crystal surface. (b) Band sketch illustrating the spin-dependent ³¹P/P_b charge carrier recombination transition. For details see text

function of the excitation lengths were carried out. Following these preparatory measurements, four experiments were performed to address the following questions:

(i) Is the EDMR signal that has previously been observed¹⁰ at magnetic fields between the two hyperfine split lines of the ³¹P for measurements conducted at X-band excitations (approx. 10 GHz) truly due to P_b states? If so, are P_b states the only interface states involved in spin-dependent transitions as illustrated in Fig. 1(b) or are there other states at or near the interface, or even in the bulk, which could contribute to the observed signals? In order to address this question, a systematic study of the EDMR spectrum (the magnetic field dependence) as a function of the interface orientation angle θ was made in order to observe all g -factors involved in spin-dependent recombination and to detect possible anisotropies of these centers.

(ii) Are the observed spin-dependent processes truly due to pairs of ³¹P and interface states as depicted in Fig. 1(b) or are the signals corresponding to different g -factors due to independent processes? In order to address this question, a series of different spin-dependent current transients was recorded under various temperatures, light intensities, surface orientations, sample voltages and offset currents as well as excitation powers and lengths. For all applied conditions, the current transients were recorded after (a) resonant excitation of the two ³¹P lines and (b) the interface states and the correlation between the dynamics of ³¹P and interface states were compared.

(iii) As an understanding about the nature of the interface defects and the transitions between interface defects and the ³¹P donor electrons was established, the main question of this study was addressed: Are the coherence times of ³¹P donors

near interface defects compromised? For this, a series of coherence time (T_2) measurements was carried out on ^{31}P donors in proximity to interface states and with the same samples, under the same conditions (in fact, during the same experimental runs), the coherence time of bulk ^{31}P was measured for comparison. For the interface T_2 measurements, modified Hahn echoes, detected with pEDMR, were used, in a similar way as recent studies of ^{31}P doped c-Si samples with (100) orientation⁶ and spin-dependent ^{31}P bulk processes at very high magnetic fields³⁷. For the bulk T_2 measurements, conventional ESR detected Hahn-echo experiments were carried out. This comparative study of T_2 times was made as a function of the temperature for $5\text{ K} \leq T \leq 13\text{ K}$.

(iv) Finally, in order to obtain information on whether the spin-coherence times T_2 of near-interface defect ^{31}P is determined by the electronic transitions between ^{31}P and interface states or by the interface defect induced spin-spin relaxation processes as suggest by de Sousa¹⁵, a comparison of electrically detected T_2 times and T_1 times was made for a temperature of $T = 5\text{L}$. In order to measure T_1 , electrically detected inversion recovery measurements were performed. To the knowledge of the authors, this is the first time that such an experiment is demonstrated.

III. EXPERIMENTAL DETAILS

For the experiments presented in the following, we used $300\ \mu\text{m}$ thick, (111) surface oriented silicon since P_b centers for this surface orientation are all identically oriented. This is in contrast to the (100) surface previously used for similar experiments^{6,10} as the (100) surface allows silicon dangling bonds (here they are called P_{b0} states) to exist in two orientations at the same time which makes their mutual EPR spectroscopic distinction as well as their distinction from other possible interface defects very difficult. The experiments were conducted with dopant concentrations of $[\text{P}] = 10^{15}\text{ cm}^{-3}$ and 10^{16} cm^{-3} which is less than 10^{17} cm^{-3} of previous EDMR studies^{6,10}. The lower concentrations ensured that interactions between neighboring ^{31}P atoms which are known to exist³⁸ at $[\text{P}] = 10^{17}\text{ cm}^{-3}$ can be neglected.

In order to enable the electrical detection of spin-coherence, the c-Si samples required contact structures which would not strongly distort the homogeneity of the spin resonant microwave fields B_1 . This problem was solved using a method similar to previous pEDMR studies at X-band^{10,39} - we designed long match-like sample substrates on which electrical sample contacts outside of the microwave field are connected to the sample via $\sim 50\text{ mm}$ long thin-film Al wires whose thickness of 100 nm is below the penetration depth of the applied microwave radiation. The contact structures were fabricated using a photo lithographical lift-off process that was carried out after the Al film was evaporated on the H-terminated silicon (111) surface of the c-Si samples that had been prepared by a wet treatment with hydrofluoric acid. In order to maximize the density of interface states, a native oxide was grown on the (111) surface after the contact deposition by exposure of the sample to ambient air.

All EDMR and EPR experiments were carried out at X-band using a cylindrical dielectric low-Q pulse resonator which was part of a Bruker Elexsys E580 EPR spectrometer. The sample temperatures were obtained with a ^4He flow cryostat, the excess charge carriers were induced through a spectral cold light source (IR and UV filtered spectral light) with an incandescent light source (Schott KL 2500 LCD) with lamp temperature of about 3000 K producing an integrated spectral intensity of approximately 5 Wcm^{-2} at the sample surface. The EDMR experiments were conducted by establishing a constant offset photocurrent using a constant current source with a time constant in excess of the experimental shot repetition time. Current transients were digitized and recorded following current amplification by a Stanford Research SR570.

The raw data recorded for the presented measurements was a combination of spin-dependent currents and microwave induced artifact currents. The latter can be recorded separately by measurement of the current response at off-spin resonant B_0 -fields. Magnetoresistance effects on the microwave induced currents can be linearly extrapolated for c-Si at the given magnetic fields. The microwave current transients obtained from this procedure were subtracted from the raw data in order to reveal the current transients solely caused by spin-dependent transitions.

IV. MEASUREMENT RESULTS

A. Identification of spin-dependent transitions

1. Experimental data

In order to confirm the results of Stegner et al.¹⁰ for a c-Si:P/SiO₂ interface with smaller ^{31}P concentration and a (111) surface orientation of the silicon sample, transient measurements of photocurrent changes ΔI were recorded under various illumination conditions and temperatures. Figure 2 displays a data set of $\Delta I(B_0, t)$ recorded as a function of the magnetic field B_0 and the time t after a 96 ns long microwave pulse with a frequency of $f = 9.749\text{ GHz}$ and a power of $P \approx 8\text{ W}$ for $T = 5\text{ K}$ and a constant photocurrent of $I = 270\ \mu\text{A}$. The sample orientation was $\theta = 0$. The data set clearly confirms the expected EPR induced currents with three local response maxima at $B_0 = 346.37\text{ mT}$, $B_0 = 347.9\text{ mT}$ and $B_0 = 350.55\text{ mT}$. The two outer peaks which are separated by a magnetic field of $\approx 4.2\text{ mT}$ are the two hyperfine lines of the ^{31}P donor electron while the peak close to the low field ^{31}P line has been attributed to interface defect states¹⁰.

2. Discussion

The transient behavior at the magnetic fields with EPR responses confirms the measurements by Stegner et al.¹⁰. It consists of a brief photocurrent quenching after the pulse, attributed to an enhancement of the interface recombination, followed by a longer-lived current enhancement. This enhancement arises because the singlet recombination rate re-

turns to its steady state faster than the resonantly quenched triplet recombination rate, causing a net quenching of the recombination rate^{10,40}. Note that variations of the temperature, the sample voltage and therefore the photocurrent as well as the illumination conditions change the quantitative dynamics of the observed transients - they do not, however, change the qualitative quenching/enhancement behavior displayed by the data set of Fig. 2, which were also observed in previously reported measurements¹⁰ on c-Si(100):P/SiO₂ with $[P] = 10^{17} \text{cm}^{-3}$.

Both the quenching and the enhancement shown in Fig. 2(d) are well fit with simple exponential decay functions, in agreement with the observation of Stegner et al¹⁰. This is somewhat counterintuitive since the random spatial distribution of the paramagnetic states involved in these transitions (see discussion in section IV B) suggests that the distances between pairs of paramagnetic states between which spin-dependent transitions occur are widely distributed. This distance distribution of states also implies a distribution of transition times⁴¹ which suggests that the observed current transients should be distributions of exponential functions for which fits with single exponentials would be poor. In contrast, observed transients are in good agreement with single exponential fits which suggests that only a narrow range of transition times exist and therefore, only pairs with a narrow range of intra-pair distances

contribute to the observed signals. We attribute the existence of a "main-pair distance" which dominates the observed signals to two factors: first, pEDMR signals vanish for pairs with very large distances (larger than the localization length of the two paramagnetic states⁴¹) as the probability for recombination is greatly diminished. Second, for very short distances, where the exchange between the two states exceeds the Larmor frequency difference within the pair⁴², the signal vanishes as the resonantly induced change of spin pair states between singlet and triplet configurations becomes increasingly forbidden⁴². Thus, there will always be a finite main-pair distance where spin-resonance induced rate changes become maximal and pairs around this distance will dominate the observed spin-dependent currents.

B. Identification of interface defects

1. Experimental data

The data presented in Fig. 2 confirms that spin-dependent interface recombination processes can be observed with pEDMR at the c-Si(111):P/SiO₂ interface which are qualitatively similar to those seen previously at the c-Si(100):P/SiO₂ interface with higher ³¹P concentration. It is therefore possible to systematically study the nature and the origin of the resonances found. Figure 3(a) displays the magnetic field dependence of the pulse induced photocurrent change $\Delta I(B_0)$ at times t after the pulse when the photocurrent changes were maximal (in the following referred to as pEDMR spectra) for five different surface orientation angles ($0^\circ \leq \theta \leq 90^\circ$) and two ³¹P concentrations. Note that while $\Delta I < 0$, the data has positive signs as each displayed spectrum was normalized to its respective extremum. The normalization was made for better comparison of the data sets since the signals obtained from samples with $[P] = 10^{16} \text{cm}^{-3}$ were significantly stronger compared to signals from samples with $[P] = 10^{15} \text{cm}^{-3}$ (note the higher relative noise in the latter spectra).

The fits of the pEDMR spectra required at least four different Gaussian peaks. A comparison with the ³¹P EPR and EDMR spectra found in the literature^{10,43} allows immediate identification of the peaks at the highest and lowest magnetic fields as the well known hyperfine split ³¹P donor electron resonances. There are at least two additional resonance signals present. As these additional peaks are very close to each other and to the low field ³¹P hyperfine resonance, significant ambiguity for the 12 fit parameters (peak centers, width, magnitude for all four lines) is present. This was overcome by a stepwise fit of the spectra: we first determine the ³¹P spectrum and subsequently fit the two remaining non-phosphorous lines (eliminating six fit parameters). The separation of the low-field ³¹P -hyperfine line from the strongly overlapping non-phosphorous lines was achieved by first fitting the high field ³¹P hyperfine peak, which has little or no overlap with the other resonances, with a single Gaussian line. From the result of this fit, we can determine both the position (assuming a hyperfine splitting of $A = 4.18 \text{ mT}$ as verified by bulk EPR measurements) and shape (assuming only negligible nuclear

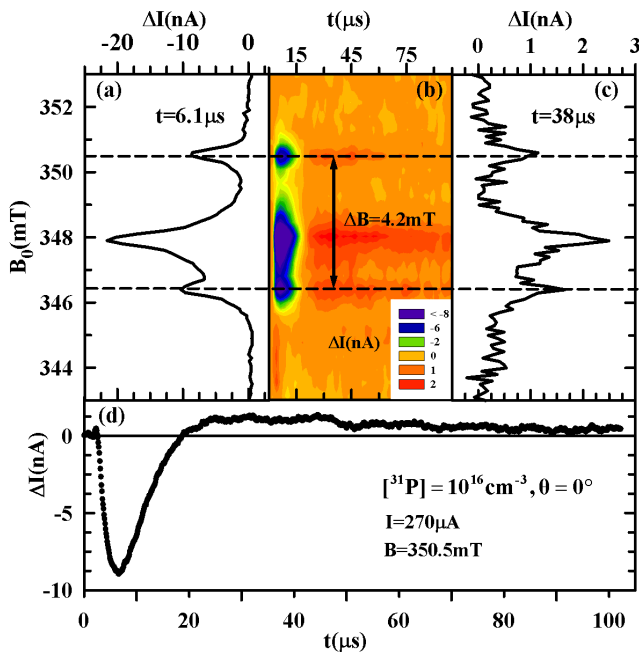


Figure 2: (color online) Plots of the microwave pulse (at $t = 0$) induced change ΔI of an interface photocurrent along a c-Si(111):P/SiO₂ interface as a function of time t and the applied magnetic field B_0 . (a,c) Plots of ΔI as functions of B_0 for the times $t = 6.1 \mu\text{s}$ and $t = 38 \mu\text{s}$, respectively, for which a quenching and an enhancement of the current changes reach their extrema. (b) color contour plot of the entire data set $\Delta I(t, B_0)$ containing the data of the plots in (a), (c) and (d). (d) Plot of ΔI as a function of the time t for a magnetic field $B_0 = 350.5 \text{ mT}$ which was on resonance with the high field ³¹P EPR line.

polarization, which is justified for the given sample temperatures and magnetic fields B_0) of the low-field ^{31}P -hyperfine peak. The residue following these fits is then able to be fit with two Gaussian resonances. The full fit, as well as the 4 constituent peaks, is shown for all spectra in Figure 3.

Figure 3(b) shows the g -factors of the non- ^{31}P lines as a function of the angle θ , obtained from the fit. It also displays a solid line which represents literature values for EPR²⁵ and EDMR^{29,31} detected P_b centers.

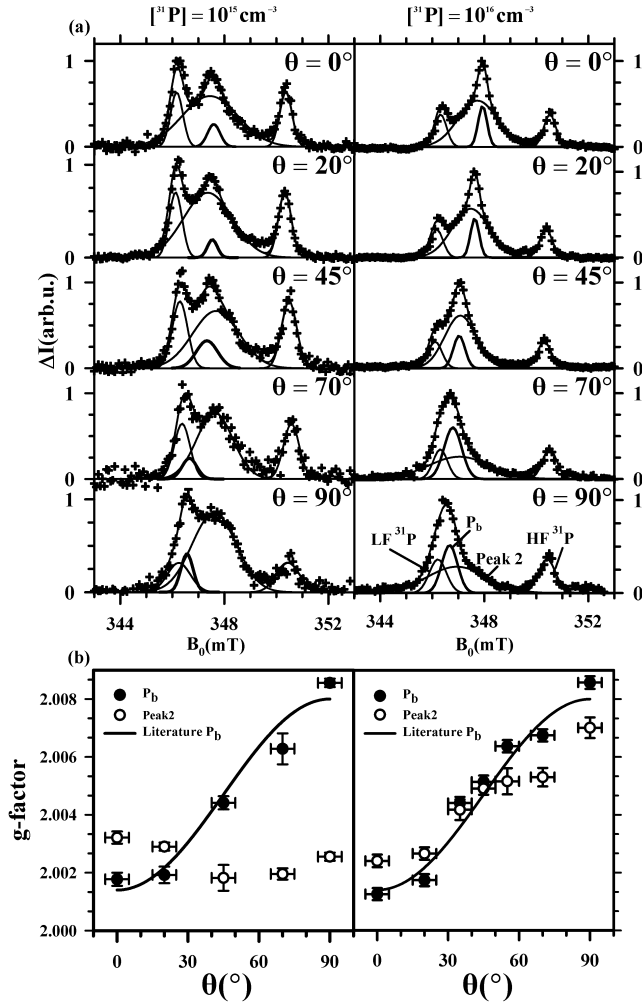


Figure 3: (a) Plots of ΔI as functions of B_0 at arbitrary times t after a microwave pulse with arbitrary length τ , frequency $f \approx 9.5$ GHz and a power $P = 8$ W and under otherwise identical conditions as for the data in Fig. 2. The data was collected for five sample orientations θ and two ^{31}P concentrations. The displayed plots are normalized to the maximum of ΔI . The solid lines represent fits of the data consisting of four Gaussian peaks, two related to the ^{31}P hyperfine line and two peaks related to interface defects. The plot for $[^{31}\text{P}] = 10^{16} \text{ cm}^{-3}$ and $\theta = 90^\circ$ has the peak assignments to the low field (LF) and high field (HF) ^{31}P resonances, the P_b peak as well as peak 2. (b) Plots of the fit results of the g -factors for the two interface defect lines as a function of θ for the two ^{31}P concentrations. The solid lines indicate the literature values for the P_b center.

2. Discussion

The anisotropy and absolute value of the g -factor of one of the two peaks is in excellent agreement with the P_b literature values for both ^{31}P concentrations. Based on this agreement, this peak can be assigned to spin-dependent transitions (recombination) which involve P_b centers. Note that previous pEDMR measurements on c-Si(111)/ SiO_2 interfaces with no ^{31}P doping have shown P_b signals^{29,31}. Since there are no ^{31}P pEDMR lines in intrinsic c-Si, it is clear that spin-dependent P_b interface recombination does not necessarily require the presence of ^{31}P atoms. Thus, the P_b involvement revealed by the data in Fig. 3 may either involve ^{31}P as illustrated in Fig. 1(b) or be due to an independent interface recombination process.

In contrast to the P_b resonance line, the assignment of the second non- ^{31}P peak (referred to as peak 2, see peak assignment in Fig. 5) is less straight forward. The fit results for $[P] = 10^{15} \text{ cm}^{-3}$ suggests that peak two is isotropic, or only weakly anisotropic, whereas the data for $[P] = 10^{16} \text{ cm}^{-3}$ is consistent with an anisotropic peak. There are two explanations for this difference between the two sets of spectra, (i) that the nature of peak 2 is different at higher ^{31}P concentrations, suggesting that the observed processes may be different and (ii) that the fit error of the center g -factor of peak 2 becomes increasingly inaccurate for larger values of θ . The latter may be due to the width of peak 2 and the relative weakness of the peak 2 intensity in comparison to the signal strengths of the P_b and ^{31}P EDMR signals at higher dopant concentrations, becoming increasingly problematic for the fit accuracy at large θ as three resonances (low field ^{31}P , P_b , peak 2) have larger overlap at higher angles. Note that the error ranges given in the plots of Fig. 3(b) are based on the uncertainty estimates of the fit routines. As additional uncertainties with regard to fit induced systematic errors are likely to exist, the true standard deviation for g -factors of peak 2 may be significantly larger. Thus, it is not clear whether the different results for g -factors of peak 2 obtained for different ^{31}P concentrations are real or fit artifacts and therefore an unambiguous statement about the anisotropy of peak 2 is not possible.

Previous pEDMR spectra on intrinsic c-Si have shown a second isotropic recombination signal with $g \approx 2.0023(6)$ ³¹. This is in good agreement with peak 2 observed on c-Si samples with $[P] = 10^{15} \text{ cm}^{-3}$. As with the previous study on intrinsic silicon, it is difficult to unambiguously assign peak 2 to a particular interface defect type. Due to its strong inhomogeneity (the large line width) and its overall magnitude in comparison to the other pEDMR lines, it is possible that peak 2 is due to one or more randomly oriented anisotropic centers whose powder spectra would cause a macroscopically isotropic wide resonance line. The g -factor and the line width are close (yet not equal) to the g -factor and line width of silicon dangling bonds in amorphous SiO_2 (so called E' centers²⁵). Thus, it is possible that the observed pEDMR data is due to transitions involving E' centers in proximity of the c-Si:P/ SiO_2 interface. Note that there are several distinct E' centers which differ by the backbonds of the Si atom on which the center is located (one or more oxygen atoms, hydrogen

atoms) or their relaxation state (the unrelaxed E' center has been called E'_δ)²⁵. Charge carrier trapping and recombination may work similarly for both the P_b centers with well defined orientation as well as the randomly oriented E' . Due to the localization length of the ^{31}P donor electron state³⁵, it is also conceivable that transitions between the shallow donor states and the deep interface states are possible. Hence, peak 2 is assigned in the following to an E' center with unspecified nature except for its proximity to the c-Si:P/SiO₂ interface.

C. Identification of ^{31}P to interface-defect transitions

1. Experimental data

The plots of Fig. 3 demonstrate the involvement of at least three qualitatively different paramagnetic electron states (^{31}P , P_b , E') in spin-dependent charge carrier recombination transitions. This observation, however, does not prove that the observed recombination transitions take place *between* these different states. While the spin-dependency of transitions through localized states requires the existence of pairs of paramagnetic states⁴⁴, there are examples of spin-dependent transitions which produce only a single resonance line in EDMR experiments^{28,39} when transitions occur between identical centers or when the paramagnetic pairs are strongly coupled. Therefore, the detection of multiple EDMR lines (as in Figs. 2 and 3) leaves the exact nature of these transitions elusive.

One approach to an understanding of whether the observed g -factors belong to the same or different transitions is to analyze the dynamics of the spin-dependent processes associated with these different resonances: Spin-selection rules usually discriminate permutation symmetries of spin $s = \frac{1}{2}$ pairs^{40,42} which means that it is the mutual orientation of the two spins, not the individual spin state of one of the two pair partners,

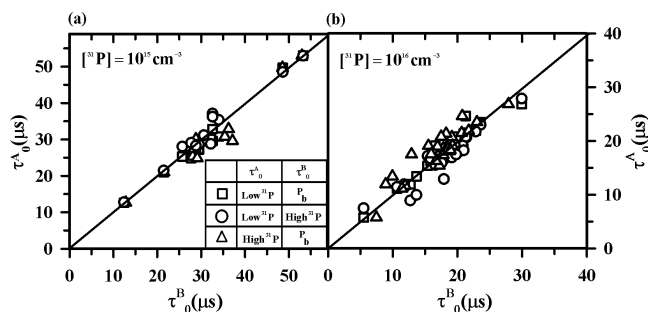


Figure 4: Plots of the zero crossing times τ_0 of magnetic resonantly induced photocurrent transients of the ^{31}P low or high field resonance (τ_0^A) versus the zero crossing times of magnetic resonantly induced current transients of the P_b / E' center resonances (τ_0^B) measured for a variety of different samples and sample conditions (temperature, offset current, illumination). The solid line is a linear function through the origin with slope 1. The two plots made for the two concentrations show a strong correlation of the zero crossing times of all three resonances.

which determines the transition rate. Therefore, the transient behavior of spin-dependent transition rates exhibits an identical behavior after a spin resonant manipulation of either one of the two pair partners. If two EDMR detected resonances exhibit a different transient behavior after the same pulsed excitation, the spin-dependent transitions corresponding to these resonances must be different as well. However, if the transient behavior is identical, the two resonances may belong to identical transitions. While different dynamics of spin-dependent transition rates for different g -factors is proof that they belong to different processes, identical transition rates only indicate that the two resonances may be due to the the same process, as they may also be due to different processes which coincidentally have the same transient behavior. Therefore, the observation of identical transients requires further testing of the correlation of the observed dynamical behavior under varying experimental conditions.

Figure 2(b) demonstrates that the fast relaxing current quenching and the slowly relaxing current enhancing behavior that is discussed above occurs similarly for both the ^{31}P hyperfine resonances and the resonances associated with interface states. The dynamics (which means the decay times of the different exponential functions), but not necessarily the absolute magnitude of current transients from different centers involved in the same electronic process are identical. Thus a comparison of different transients yields information about the paramagnetic centers between which transitions take place. We compare the "zero-crossing time", τ_0 , defined as the time after the pulsed excitation of a spin-resonance induced current transient when the quenching and enhancement are identical. The comparison as shown in Fig. 2(b) clearly reveals identical $\tau_0 \approx 18 \mu\text{s}$ with an error of $\approx 1 \mu\text{s}$. This suggests that the processes connected to these resonances are due to transitions involving both the ^{31}P donor states as well as the P_b interface state or the E' near-interface state in the way depicted in the sketch of Fig. 1(b).

In order to test whether τ_0 for the interface defects and the ^{31}P remained identical when the dynamics of the spin-dependent current signal is changed, the experiment presented in Fig. 2(b) was repeated under various combinations of temperatures (5 K, 8 K, 10 K, 13 K and 15 K), sample currents (10 μA ~ 300 μA (and therefore different electric fields), and sample surface orientations for the two different ^{31}P doping concentrations mentioned above. Due to the variation in charge carrier concentration as well as Fermi- and quasi-Fermi energies caused by changing these experimental parameters, the dynamics of the observed spin-dependent recombination transitions, and therefore the dynamics of the observed current signals, changed significantly between measurements. For all data sets, τ_0 was determined for transients recorded at magnetic fields corresponding to the two ^{31}P hyperfine resonances as well as at the maximum of the overlapping interface defect signals. The results of this procedure are displayed in Fig. 4 in two correlation graphs, for samples with the two different donor concentrations. Each graph displays a plot of τ_0^A versus τ_0^B with A and B corresponding to the ^{31}P low field and the ^{31}P highfield resonances, respectively (represented by the circles) the ^{31}P low field and the interface state resonances, re-

spectively (represented by the squares) and the ^{31}P high field and the interface state resonances, respectively (represented by the triangles).

2. Discussion

The data in Fig. 4 reveals three observations:

(i) As anticipated, the variation of experimental parameters clearly varies the dynamics of the observed signals.

(ii) While similar combinations of experimental parameters were used for the two concentrations, the times τ_0 of the samples with $[\text{P}] = 10^{15} \text{ cm}^{-3}$ are generally slower than the τ_0 obtained for $[\text{P}] = 10^{16} \text{ cm}^{-3}$. This observation shall not be discussed quantitatively in the following, however, it is conceivable that as an increase of the ^{31}P doping concentration leads to a smaller main-pair distance (note the definition of main-pair distance given in section IV A 2) for ^{31}P to interface defect pairs as well as ^{31}P to ^{31}P pairs. It should not lead to a change of the main-pair distance of interface defect pairs. The observed general decrease of the transition time with an increase of the ^{31}P concentration therefore suggests that the observed signals are predominantly due to transitions involving ^{31}P and not transitions between two interface defects. We note that there may be other reasons for this decrease in transition times with increasing doping density: one such possibility is that different internal fields may lead to different energy separations between pair partners with different intra-pair distance, with a corresponding change in transition probability.

(iii) The entire set of data reveals a strong correlation of τ_0 between any combination of signals, whether it is between the two ^{31}P hyperfine signals or between the interface signals and either one of the two ^{31}P hyperfine signals. The correlation between the two ^{31}P hyperfine peaks is expected as the only difference between ^{31}P atoms contributing to these two peaks is the nuclear spin state, which has little influence on electronic transition times. The strong correlation between any two of the ^{31}P peaks and the interface states is again strong evidence that the spin-dependent transitions measured involve ^{31}P -interface defect pairs in the way sketched in Fig. 1(b).

It was not possible to obtain unambiguous correlation plots similar to those in Fig. 4 for the two different interface and near-interface defects discussed above. It is therefore not possible to verify whether the observed correlation between the ^{31}P and the interface defects applies to both interface centers or only to the one which dominated under the observed conditions. However, we point out that the strong correlation seen in the plots of Fig. 4 is consistent with the assumption that the dynamics of both defects correlates with the ^{31}P dynamics and thus, spin-dependent recombination through both interface defects in the manner sketched in Fig. 1(b) seems possible.

The correlation data of Fig. 4 raises a question about the presence of spin-dependent transitions between interface defects. It is known from previous pEDMR studies of (111) oriented nominally intrinsic c-Si/SiO₂ interfaces at X-Band^{29,30,31}, as well as from recent pEDMR studies at high magnetic fields ($\approx 8.5\text{T}$)²⁸, that spin-dependent transitions

involving only interface defects but not ^{31}P are possible and that these transitions can be due to spin-dependent resonant tunnelling between two interface states in sufficient spatial and energetic proximity. We conclude from the data seen in Fig. 4 that, whilst such interface defect-only processes may or may not have been present at the investigated c-Si:P/SiO₂ interfaces, they did not dominate the observed spin-dependent rates, consistent with the very weak signal strength of previous pEDMR measurements on intrinsic c-Si/SiO₂ interfaces conducted at X-Band³¹. The interface defect signals are weak in spite of the presence of a significantly higher interface defect density compared to the areal density of ^{31}P close to the interface. This may be explained by considering the signal from interface defect pairs, which have almost identical g-factors and therefore stronger coupling, leading to lower pEDMR signals than those seen from ^{31}P -defect pairs which have quite different g-factors and weaker, but still finite, coupling⁴², and therefore dominate the signal.

D. Electrical detection of spin coherence

1. Experimental data

The ability to perform spin-Rabi nutation is a crucial prerequisite for the coherence time measurements using echo pulse sequences as it reveals the resonantly induced Rabi frequency for a given set of experimental conditions (e.g. for the applied microwave power). The Rabi frequency is needed to determine the pulse lengths required to obtain the correct nutation angles during the pulse sequences. We performed transient nutation style experiments for the electrical detection of spin-Rabi nutation. For these measurements, the photocurrent change ΔI was integrated between two appropriately chosen integration times t_1 and t_2 after the microwave pulse so we obtain a charge

$$Q = \int_{t_1}^{t_2} \Delta I(t) dt \quad (1)$$

that is proportional to the number of spin-dependent transitions induced by the resonant excitation⁴². As Q is proportional to the projection of the resonantly prepared coherent spin state $|\psi(\tau)\rangle$ at the end of the excitation pulse of length τ onto the singlet state $|S\rangle$ ^{10,40}, the measurement of $Q(\tau) \propto |\langle S|\psi(\tau)\rangle|^2$ reveals the propagation of the singlet content of $|\psi(\tau)\rangle$ during the pulse in a transient nutation-style experiment. Figure 5(a) displays the measurement of $Q(\tau, B_0)$ as function of the pulse length τ and the magnetic field B_0 for a c-Si sample with $[\text{P}] = 10^{16} \text{ cm}^{-3}$, a temperature $T = 5 \text{ K}$, $\theta = 90^\circ$, and integration times $t_1 = 6 \mu\text{s}$ and $t_2 = 16 \mu\text{s}$.

2. Discussion

The data set displayed in Fig. 5 shows that $Q(\tau)$ has an oscillating behavior around the same magnetic fields which produced local current response maxima in the data set displayed in fig. 2. The oscillatory dependence on τ is due to the

dephasing spin–Rabi nutations as demonstrated, for the magnetic field $B_0 = 348$ mT, by the data sets displayed in Fig. 5(b): The three plots show $Q(\tau)$ for three different microwave powers (B_1 field strengths). We anticipate⁴⁰ the spin–Rabi nutation signal of an inhomogeneously broadened spin ensemble to follow the integral of a first kind Bessel function

$$Q(\tau) \propto \int_0^{\gamma B_1 \tau} J_0(2x) dx = \frac{1}{\pi} \int_{-\infty}^{\infty} \frac{\sin^2(\gamma B_1 \tau \sqrt{1+x^2})}{1+x^2} dx \quad (2)$$

in which $\gamma \approx 2.8$ MHz is the gyromagnetic ratio. A fit of the three data sets in Fig. 5(b) with Equ. 2 shows a good agreement and it reveals values for the nutation frequencies $\Omega_R = \gamma B_1$ for the three different powers. A plot of Ω_R versus the B_1 fields obtained from the relative microwave attenuation used for the three measurements shows that the expected linearity of the spin–Rabi nutation is given. The data shown in Fig. 5 is thus shown to be due to the spin–Rabi nutation of ^{31}P

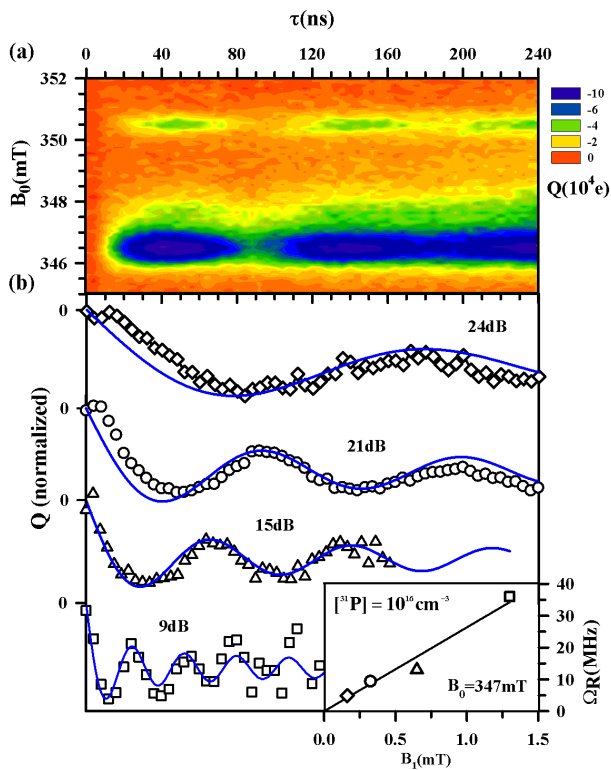


Figure 5: (color online) (a) Plot of the measured integrated charge $Q(\tau, B_0)$ as defined by Equ. 1 as a function of the magnetic field B_0 and the length τ of an applied microwave pulse with frequency $f = 9.7475$ GHz and power $P = 8$ W. (b) The symbols represent a plot of the measured charge $Q(\tau)$ for four different microwave powers at $B_0 = 347$ mT. Note that for the latter case, the pulse length was recorded up to $\tau = 120$ ns only as the measurement was limited by signal perturbation due to the pulse induced microwave current artifacts. The blue lines represent fits of an integrated Bessel function to the experimental data. The Rabi–nutation frequencies obtained from these fits are displayed in the inset as a function of the applied B_1 field. The fit of a linear function through the origin (black line) shows good agreement.

donor and interface electron spins, confirming the previously reported observation made for c-Si(100):P/SiO₂ interface with higher ^{31}P concentration. Note that with the data obtained from the transient nutation measurement, it is possible to determine the length of π - and $\frac{\pi}{2}$ -pulses as needed for the T_2 measurements in the following. The latter will be necessary since the decay of the Rabi nutation as displayed in Fig. 5 is not a measure for spin–coherence. The agreement of the nutation data with the integrated Bessel function is indicative of coherent dephasing, not coherence decay, being the dominant source of the observed nutation decay. This assumption is confirmed by the electrically and pEPR detected echo data discussed below which shows that the real T_2 spin coherence time of the ^{31}P donor electrons is distinctively longer than the decay of the nutation signal.

E. Comparison of the coherence time T_2 of ^{31}P donor electrons at the c-Si:P/SiO₂ interface and in the c-Si:P bulk

1. PEDMR and pEPR detected spin–echoes

The data presented in sections IV A and IV C showed that the spin–dependent current observed at c-Si:P/SiO₂ interfaces are due to transitions that take place between ^{31}P donor electron states and c-Si:P/SiO₂ interface states in their proximity. A measurement of the ^{31}P donor electron spin coherence time (the T_2 time) using pEDMR will therefore reveal only the T_2 of ^{31}P donor electrons in close proximity of the c-Si:P/SiO₂ interface defects. In contrast, a T_2 measurement using conventional radiation detected pEPR will reveal the coherence time of ^{31}P donors in the bulk as the contribution of near–surface ^{31}P atoms in the pEPR signal will be negligible in comparison to the magnitude of the bulk ^{31}P signal. Thus, the comparison of T_2 times measured by pEDMR and pEPR allows the influence of interface defects on the ^{31}P donor electron spin coherence times to be studied.

The pEPR and pEDMR experiments require different approaches to the measurement of T_2 times: With pEPR, the T_2 times of paramagnetic centers can be determined most easily using a Hahn–echo pulse sequence. Hahn–echoes are a temporary rephasing of a spin–ensemble due to a pulse sequence consisting of an initial $\pi/2$ -pulse which turns the ensemble polarization into the plane perpendicular to the B_0 field and a subsequent π -pulse which initiates the phase reversal⁴⁵. As illustrated in the inset sketch of Fig. 6(b), when the echo pulse sequence consists of the $\frac{\pi}{2} - \pi$ pulses with a duration τ between the pulses, a Hahn–echo can be observed at a time τ after the second pulse which is the time 2τ after the first pulse. When a Hahn–echo is observed, T_2 -times can be measured by determining the decay of the Hahn–echo as a function of twice the pulse separation time 2τ . Figure 6(b) shows a data set for a Hahn–echo transient obtained from a ^{31}P doped c-Si sample with $[^{31}\text{P}] = 10^{16} \text{ cm}^{-3}$ at a temperature $T = 10$ K and with $\theta = 90^\circ$. One can clearly see a local maximum of the transient microwave signal at a time $t = 2\tau$. The data set was well fit by a Gaussian function which was used in order to determine the integrated intensity of the echo.

In contrast to pEPR measurements, pEDMR does not allow direct observation of Hahn–spin echoes through real time transient measurements as the integrated sample current $Q(\tau)$ always represents a projection of the spin–state at the end of the pulse sequence onto a singlet state. Therefore, the T_2 time measurement using pEDMR requires the utilization of a modified Hahn-echo pulse sequence that is illustrated in the inset of Fig. 6(a)⁶. In order to resolve the dynamics of the spin–ensemble during and after the $\frac{\pi}{2} - \pi$ pulse sequence, a third pulse with length $\frac{\pi}{2}$ is applied at a time τ' after the begin of a conventional Hahn-echo pulse sequence. The third pulse projects the spin–ensemble at the time τ' onto the \hat{z} -direction which in turn determines the singlet content of the ^{31}P –interface defect pair. The charge Q integrated following this pulse therefore represents the polarization of the spin–ensemble along the \hat{x} - axis [\hat{y} -axis] at the time τ' (assuming the B_1 field is directed along the \hat{y} - axis [\hat{x} - axis]). The measurement of the entire echo transient using the pEDMR detection requires repetition of the echo sequence for various τ' : the third pulse (also called the detection pulse) is swept through the time range which covers the Hahn–echo maximum as well as the echo baseline. While this procedure makes the time needed for T_2 measurements significantly longer, it allows the measurement of a T_2 using pEDMR. The plot displayed in Fig. 6(a) shows an electrically detected spin–echo measured on the same sample and under identical conditions, recorded during the same experimental run as the measurements shown in Fig. 6(b). The data clearly shows the echo whose fit with a Gaussian function is displayed by the solid line. The comparison of the two echo functions shows that the electrically detected echo is more narrow than the radiation detected indicating that it is due to a more heterogeneous spin ensemble.

The use of two different measurement techniques (pEDMR, pEPR) raises the question of whether both methods probe the same observable, namely the T_2 of ^{31}P impurity atoms. There has recently been a comparative study of T_2 times confirming this identity using a pEDMR detected spin–dependent bulk process³⁷ (a spin-trap process of ^{31}P in c-Si that becomes rele-

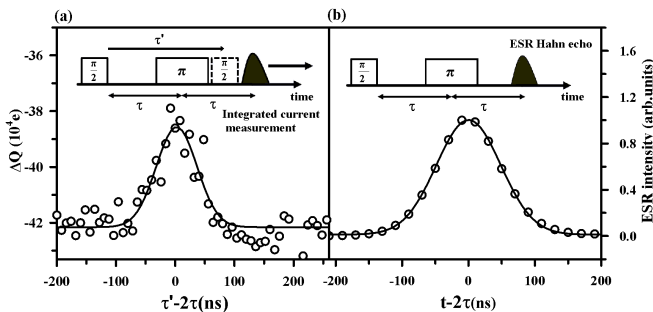


Figure 6: Comparison of (a) an electrically detected spin–echo with $\tau = 300$ ns and (b) a conventional radiation detected Hahn–echo with $\tau = 10$ μs . The data sets were recorded on the same sample, under identical sample conditions ($T = 10$ K, $I = 250$ μA , $\theta = 90^\circ$) during the same experimental run. Both data sets were fit with Gaussian functions (solid line). Insets of the two plots show sketched timelines of the used pulse sequences.

vant at high magnetic fields) which showed that both pEDMR and pEPR measured T_2 times reveal an excellent agreement. Thus, in the following, systematic measurements comparing pEPR detected T_2 -times of ^{31}P bulk impurities and pEDMR detected T_2 -times of ^{31}P interface impurities are presented. These measurements are made for three reasons: (i) To extend the previous observation of electrically detected Hahn-echoes⁶ to c-Si(111) surfaces. (ii) To measure the temperature dependence of the T_2 -times. (iii) To obtain comparable measurements with both pESR and pEDMR under identical conditions.

2. Measurement of spin–echo decays

The spin–echo effects shown in Fig. 6 are imprints of coherent spin motion on currents or radiation intensities. When a spin ensemble loses coherence during a $\frac{\pi}{2} - \pi$ sequence, the intensity of the spin–echo following this sequence decays. Quantifying the decay of Hahn–echoes is a direct measure of the coherence time T_2 ⁴⁵. Figure 7 displays a set of electrically detected Hahn echoes as well as a plot of the integrated echo intensities obtained from them, recorded on a sample with $[\text{P}] = 10^{16}$ cm^{-3} at magnetic fields in resonance with the high field ^{31}P peak at $T = 10$ K and $\theta = 90^\circ$, and with a sample current of $I = 250$ μA . One can clearly see the gradual decay of the echo intensity with increasing pulse separation time τ . The solid line of the plot in Fig. 7 displays a fit of the intensity data with a modified exponential function

$$I(2\tau) = e^{-\frac{2\tau}{T_2} - \frac{8\tau^2}{T_2^2}} \quad (3)$$

which contains a contribution due to a single exponential T_2 decay as well as the stretched exponential contribution due to the isotopical influence of the ^{29}Si which causes spin–diffusion with time constant T_5 ^{7,37}. The plot in Fig. 7 exhibits a good agreement of the echo decay with the fit function and thus, by using this method for both pEDMR as well as pEPR detected echo decay measurements, the T_2 times of ^{31}P impurities can be determined for the c-Si:P bulk and the c-Si:P/SiO₂ interface, respectively. Note that all pESR detected and most pEDMR detected echo measurements were conducted on the low field peak of the hyperfine split ^{31}P resonance. In order to confirm that the spectral proximity of the P_b –peak to the low field ^{31}P resonance under the given experimental conditions does not distort the electrical T_2 measurements, control measurements were carried out on the high field ^{31}P peak for $T = 5$ K. Within the given error margins, the results of these control measurements (Fig. 8, blue solid diamonds) are in agreement with the measurements obtained from the low field ^{31}P resonance.

3. Temperature dependence of T_2 times

The measurement of T_2 as described above was repeated on the same sample with pEPR at temperatures $T = 5$ K, 8 K, 10 K, 11 K, 12 K, 13 K, 15 K and with pEDMR at temperatures

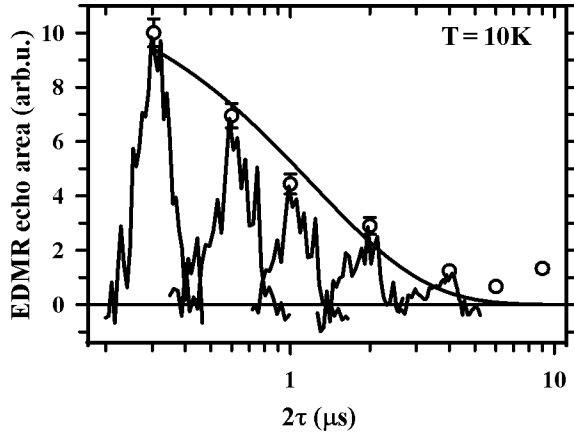


Figure 7: Plot of integrated intensities of the electrically detected echoes as a function of 2τ recorded with pEDMR on a c-Si:P/SiO₂ sample with $[P] = 10^{16} \text{ cm}^{-3}$. The solid line represents a fit with a modified multiexponential decay function (see text), the small inset plots represent plots of echo data sets.

of $T = 5 \text{ K}, 10 \text{ K}, 13 \text{ K}$. The integrated echo intensities of these measurements are plotted in Fig. 8 along with the results of their fit with Eqn. 3. The comparison of the pEDMR and the pEPR data sets shows that while there is a strong temperature dependence of the echo decay for the pEPR data, the pEDMR decay is faster and, within the range $T = 5 \text{ K}$ to 13 K , nearly constant. In order to analyze these observations quantitatively, the fit results for T_2 are plotted for both the pEDMR and the pEPR measurements in an Arrhenius plot in Fig. 9.

The coherence time of the bulk ^{31}P donors, T_2 , determined via pEPR, is well fit with a function of the form:

$$\frac{1}{T_2} = A e^{\frac{-\Delta E}{k_B T}} + \frac{1}{T_0} \quad (4)$$

where ΔE is an activation energy, and $1/T_0$ a constant relaxation rate independent of temperature. The best fit occurs with $\Delta E = 9.1 \pm 0.5 \text{ meV}$ and $1/T_0 = 10 \pm 1 \text{ kHz}$.

4. Discussion

As the pEDMR and the pEPR data displayed in Fig. 9 was collected on the same sample in the same experimental run, it is clear that the pEDMR measured T_2 times of ^{31}P donor spins in close proximity to interface defects are significantly shorter than the pEPR measured T_2 times and, within the error, independent of the temperature. At the same time, the pEPR measured T_2 of the bulk ^{31}P donor spins is not only longer than the pEDMR measured ^{31}P donor spins, it is also highly temperature dependent. In the temperature range from $T = 5 \text{ K}$ to 15 K , the coherence time changes by about a factor 50, exhibiting a good agreement with the previously demonstrated thermal activation⁷ of ^{31}P in a c-Si environment with a natural abundance of the ^{29}Si isotope. The comparison of T_2 of ^{31}P in proximity to interface defects with those in the bulk therefore shows that interface defects significantly

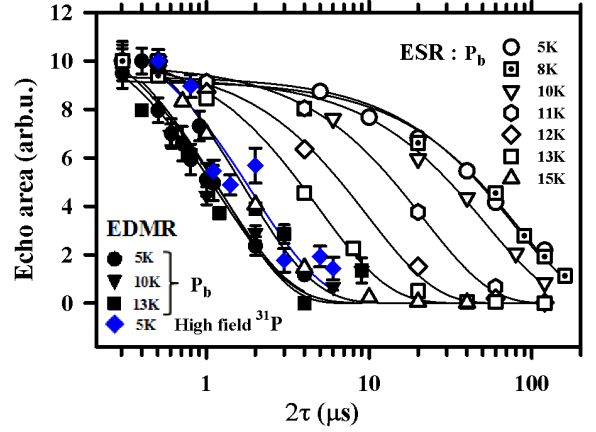


Figure 8: (color online) Plot of the normalized integrated echo intensity of pEPR and pEDMR detected Hahn echoes as a function of the logarithms of the pulse separation time τ for various temperatures. The data sets were fit with the modified exponential function given by Eqn. 3. All pEDMR and pEPR measurements were conducted on the same samples during the sample experimental run.

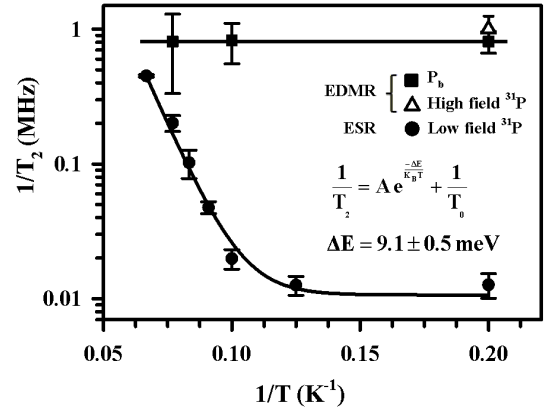


Figure 9: Plot of the logarithm of coherence decay rate T_2^{-1} obtained from the data shown in Fig. 8 as a function of the inverse temperature T^{-1} . The solid lines are fits of the data. The pEDMR data is fit with a constant function. The pEPR is fit with a combination of a constant function and a temperature activated Boltzmann factor.

shorten the donor electron spin coherence time. Within the given temperature range, T_2 appear to be pinned at $\approx 1.3 \mu\text{s}$, a value which has been observed previously for electrically detected ^{31}P spins in c-Si samples with different surface orientations, donor concentrations and experimental conditions^{6,10}. The independence of the donor spin coherence time of near-interface defect ^{31}P atoms from experimental conditions, including temperature, suggests that in contrast to bulk donors, T_2 of the near-surface donors is not determined by spin-spin or spin-lattice interactions but by transition directly related to the interface defects in their immediate proximity.

We identify two possible origins for the drastic quenching of the ^{31}P donor electron spin T_2 time in proximity of interface defects described above:

(i) The electronic transition between the ^{31}P donor state and the P_b center. This occurs when the donor electron falls into the doubly occupied interface ground state. The electronic transition leaves both the ^{31}P donor and the interface state diamagnetic since there is no donor spin present after the transition and the interface state is a doubly occupied singlet state.

(ii) A fast T_2 of the interface state which significantly quenches the T_2 relaxation of ^{31}P donor spins in its proximity as suggested by de Sousa¹⁵.

Note that the electronic transition is a limitation to both T_1 as well as T_2 processes of the spin pairs as it destroys the pairs and when the electronic transition is the limiting factor for the T_2 times, both, the electrically measured T_2 and T_1 times should be equal. In contrast, it is conceivable that the interface state induced enhancement of the ^{31}P T_2 relaxation keeps the T_1 either unchanged or significantly slower than the T_2 time. As a consequence, if the electronic transition time is longer than the P_b induced T_2 time, the electrically measured T_1 time equals the electronic transition time and it should therefore be significantly longer than the electrically measured T_2 times. Hence, a study of T_1 times of the near-interface defect ^{31}P donor electron spins, as presented in the following, has been conducted.

F. Comparison of T_2 and the longitudinal relaxation time T_1 of ^{31}P donor electrons at the c-Si:P/SiO₂ interface

1. Electrical detection of spin inversion

In order to probe T_1 of near-interface ^{31}P , electrically detected inversion recovery experiments were carried out for a temperature of $T = 5\text{K}$ where pESR measurements of bulk ^{31}P donor spins reveal large differences between T_1 and T_2 times⁷. The idea behind the inversion recovery experiment⁴⁵ is to invert a given spin polarization towards a negative non-equilibrium polarization and to then observe transiently the gradual return toward the equilibrium due to T_1 processes. Thus, the experiment consists of an initial inversion pulse, a defined delay time τ'' during which the spin ensemble undergoes T_1 relaxation and a subsequent polarization measurement which is typically conducted by utilization of a Hahn-echo sequence with fixed pulse separation time τ . Figure 10 displays a sketch of the pulse sequence used for the electrical inversion recovery measurements presented in the following. Similar to the Hahn-echo decay measurements, the Hahn-echo is measured with pEDMR by repetition of the experiment whilst applying projection pulses which are gradually swept through the echo sequence. The data in Fig. 10 shows an inverted Hahn-echo recorded with a short $\tau = 252\mu\text{s}$ and an equally short delay time $\tau'' = 52\text{ns}$ producing strong inversion. Instead of the positive spin echo as detected for a simple Hahn-echo sequence, the sign of the echo is negative. To the knowledge of the authors, the data shown in Fig. 10 is the first demonstration of an electrically detected spin inversion experiment.

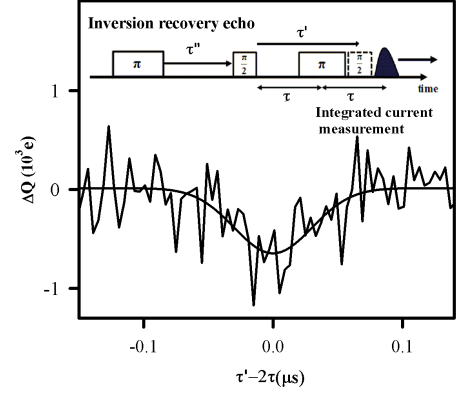


Figure 10: Demonstration of an electrically detected spin inversion recovery experiment. The inset is a sketch of the inversion recovery pulse sequence which consists of the Hahn-echo sequence that is preceded by an inversion (π -) pulse at a time τ'' before the Hahn-echo sequence begins. Similar to the electrically detected Hahn-echo shown in Fig. 6, a projection pulse is shifted through the sequence during different repetitions of the experiment. The main plot displays an echo recorded by plotting Q as a function of the difference $\tau' - 2\tau$ between the projection pulse begin τ' and the echo maximum at 2τ .

2. Inversion recovery of near-interface defect ^{31}P donor electrons

In order to determine T_1 , the experiment shown in Fig. 10 was repeated for seven values of τ'' in the range of $52\text{ns} \leq \tau'' \leq 20\mu\text{s}$. The results of these experiments are displayed in Fig. 11. They show that the polarization inversion that exists directly after the inversion pulse (τ'' is very small) exponentially approaches the steady state polarization with increasing τ'' . The integrated echo amplitudes were obtained from a fit of the echo data with Gaussian functions. They dependence on τ'' show an excellent agreement with an exponential decay function with a negative offset

$$M(\tau'') = M(0) \left[1 - 2e^{-\frac{\tau''}{T_1}} \right] \quad (5)$$

The time constant $T_1 = 4.0(5)\mu\text{s}$ obtained from this fit is more than six orders of magnitude shorter than the previously investigated bulk T_1 times⁷ which shows that the proximity of P_b centers leads to dramatically reduced T_1 times.

3. Discussion

The measurement of T_1 of ^{31}P donor electrons in proximity of interface defects revealed a T_1 time which was quenched by orders of magnitude compared to bulk ^{31}P : However, in contrast to bulk pESR measurements, T_1 is only about a factor 3 longer than the electrically detected T_2 time at the measured temperature of $T = 5\text{K}$. Following the argumentation given in section IVE 4, we learn that since $T_2 < T_1$, T_1 will be determined by the electronic transition but not T_2 as it is faster due to the influence of the nearby interface defect. It shall be emphasized though that the errors of the T_1 and T_2 measurements have been deduced from the fits of the Hahn-echo and

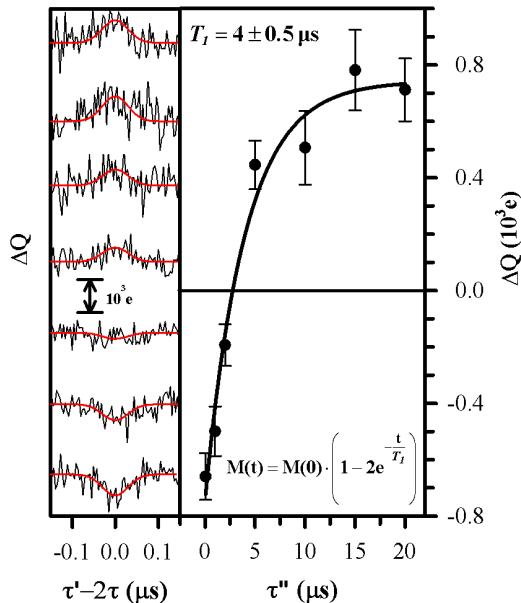


Figure 11: (color online) Plot of the integrated echo intensity detected with the pulse sequence shown in Fig. 10 as a function of the inversion recovery time τ'' . The solid line represents a fit of the data with a single exponential function. Note that the inverted echo for small τ'' changes into a non-inverted echo with equal magnitude for large τ'' . The inset plots on the left show the raw data of the various echo measurements as well as fits with Gaussian functions which are the basis for the integrated echo intensities.

inversion recovery data with eqs. 3 and 5, respectively which leaves a significant uncertainty regarding the magnitude of the measured T_1 and T_2 times. Given the proximity of the two values within the calculated errors and the remaining uncertainty about the given errors, it can not be absolutely excluded that $T_1 \approx T_2$. The latter would be indicative that the electronic transition not only determines T_1 but also T_2 . Note that in spite of this uncertainty, it is clear that the electronic transition can not be slower than the measured T_1 -time and it can not be faster than the measured T_2 -time. Hence it is unambiguously clear that the ^{31}P -interface defect process takes place on a time scale in the lower microsecond range ($1\mu\text{s} - 4\mu\text{s}$).

V. CONCLUSIONS

The realization that T_1 and T_2 times of ^{31}P donor electron spins near-c-Si:P/SiO₂ interface defects are drastically shortened to a similar value is proof that the recombination of the ^{31}P donor electron into a charged interface ground state is the lifetime limiting process of the ^{31}P qubit. This conclusion is also supported by the independence of the transition time on the temperature as this suggests that the observed spin relaxation times are determined by the ^{31}P -P_b pair geometry and not phonon density. This conclusion is also consistent with the assumption that only pairs with a certain, narrowly distributed "main" distance contribute to the observed pEDMR signals.

Our results have implications for proposed mechanisms to readout donor spins using nearby probe spins, particularly interface defects. Without the ability to vary the coupling between donor and probe spins, the electronic transition times will be fixed, limiting T_2 and also limiting the readout time. To overcome this problem, control of the coupling between target and probe spins will be required. This may be achievable using the Stark effect as electric fields will have a stronger effect on the localization of the slightly delocalized ^{31}P donor wave function in comparison to the extraordinary strongly localized deep interface defects. Whether these different electric field sensitivities have a significant impact on the exchange coupling between the ^{31}P donor interface states in close proximity at sufficiently low fields remains to be proven.

The data presented and discussed above strongly supports the model for spin-dependent recombination via ^{31}P donors and interface defects that was presented by Stegner et al.¹⁰. Whilst this explanation for the observed EDMR signal has become commonly accepted, and is further supported by the results presented here, the possibility remains that other processes also contribute to the resonant changes in current. Given the now significant evidence supporting the ^{31}P -P_b model^{6,10,27}, we agree with the conventional understanding and conclude here that we are indeed observing spin dependent transitions between ^{31}P donors located close to P_b defects at the Si(111)-SiO₂ interface.

Finally, we note that the effect of spin-dependent transitions in reducing coherence times may not be restricted to the mechanisms presented here, but may also be important for other mechanisms, such as spin dependent scattering of conduction electrons by donor spins in two dimensional electron gasses^{46,47,48,49,50}.

VI. SUMMARY

In summary, we have reported on the investigation of spin-dependent processes at the c-Si:P/SiO₂ interface using pEDMR, and shown that spin-dependent ^{31}P to interface defect recombination takes place at the c-Si (111) surface in a similar way as previously described processes for c-Si(100) surfaces. The imprints of spin-dependent recombination on interface currents reveal EPR resonances of the hyperfine split ^{31}P resonance and P_b defects and at least one other defect, assigned here to the unrelaxed E' defect in the SiO₂ matrix, previously unobserved in ^{31}P doped samples. The correlation measurements of the dynamics of these pEDMR detected signals strongly support the model that recombination transitions between ^{31}P and the interface defect states occur. By electrical detection of spin-echoes, a measurement of both the coherence time T_2 as well as the longitudinal relaxation time T_1 of ^{31}P donor spins in proximity to interface defects was possible. These measurements revealed that $T_2 \approx 1.3\mu\text{s}$ independent of the applied temperature range for $5\text{K} \leq T \leq 13\text{K}$. The longitudinal relaxation time $T_1 \approx 4\mu\text{s}$ at $T = 5\text{K}$. The observations contrast the pESR measured T_1 and T_2 of bulk ^{31}P which are significantly longer and strongly temperature dependent. Our observation show that the proximity of interface

defects to ^{31}P donors introduces spin-dependent recombination and that these electronics transitions significantly limit both, the phase coherence time T_2 as well as the longitudinal relaxation time T_1 of donors near interface defects. The implications of these findings for possible applications of the ^{31}P

-interface defect transition as spin ^{31}P readout for proposed potential spin electronics or quantum information applications have been discussed.

-
- * Electronic address: dane.mccamey@physics.utah.edu
 † Electronic address: boehme@physics.utah.edu
- ¹ G. Feher and E. A. Gere, *Phys. Rev.* **103**, 501 (1956).
 - ² G. Feher, *Phys. Rev. Lett.* **3**, 135 (1959).
 - ³ I. Appelbaum, B. Huang, and D. J. Monsma, *Nature* **447**, 295 (2007).
 - ⁴ B. E. Kane, *Nature* **393**, 133 (1998).
 - ⁵ R. G. Clark, R. Brenner, T. M. Buehler, V. Chan, N. J. Curson, A. S. Dzurak, E. Gauja, H. S. Goan, A. D. Greentree, T. Hallam, et al., *Philosophical Transactions of the Royal Society of London Series A - Mathematical Physical and Engineering Sciences* **361**, 1451 (2003).
 - ⁶ H. Huebl, F. Hoehne, B. Grolik, A. R. Stegner, M. Stutzmann, and M. S. Brandt, *Phys. Rev. Lett.* **100**, 177602 (2008).
 - ⁷ A. Tyryshkin, S. Lyon, A. V. Astashkin, and A. M. Raitsimring, *Phys. Rev. B* **68**, 193207 (2003).
 - ⁸ J. J. L. Morton, A. M. Tyryshkin, R. M. Brown, S. Shankar, B. W. Lovett, A. Ardavan, T. Schenkel, E. E. Haller, J. W. Ager, and S. A. Lyon, *Nature* **455**, 1085 (2008).
 - ⁹ C. Boehme and K. Lips, *physica status solidi B* **233**, 427 (2002).
 - ¹⁰ A. R. Stegner, C. Boehme, H. Huebl, M. Stutzmann, K. Lips, and M. S. Brandt, *Nature Physics* **2**, 835 (2006).
 - ¹¹ T. M. Buehler and V. Chan, A. J. Ferguson, A. S. Dzurak, F. E. Hudson, D. J. Reilly, A. R. Hamilton, R. G. Clark, D. N. Jamieson, C. Yang, C. I. Pakes, S. Prawer, *Appl. Phys. Lett.* **88**, 192101 (2006).
 - ¹² V. C. Chan, T. M. Buehler, A. J. Ferguson, D. R. McCamey, D. J. Reilly, A. S. Dzurak, R. G. Clark, C. Yang and D. N. Jamieson, *Appl. Phys. Lett.* **88**, 192101 (2006).
 - ¹³ T. Schenkel, J. Liddle, J. Bokor, A. Persaud, S. Park, J. Shangkuan, C. Lo, S. Kwon, S. Lyon, A. Tyryshkin, et al., *Microelectronic Engineering* **83**, 1814 (2006).
 - ¹⁴ T. Schenkel, A. M. Tyryshkin, R. de Sousa, K. B. Whaley, J. Bokor, J. A. Liddle, A. Persaud, J. Shangkuan, I. Chakarov, and S. A. Lyon, *Applied Physics Letters* **88**, 112101 (2005).
 - ¹⁵ R. de Sousa, *Phys. Rev. B* **76**, 245306 (2007).
 - ¹⁶ G. Lucovsky, Y. Wu, H. Niimi, V. Misra, and J. C. Phillips, *Applied Physics Letters* **74**, 2005 (1999).
 - ¹⁷ K. Eng, R. N. McFarland, and B. E. Kane, *Appl. Phys. Lett.* **87**, 052106 (2005).
 - ¹⁸ K. Eng, R. N. McFarland, and B. E. Kane, *Phys. Rev. Lett.* **99**, 016801 (2007).
 - ¹⁹ Y. Nishi, *Jpn. J. Appl. Phys.* **10**, 52 (1971).
 - ²⁰ E. H. Poindexter, P. J. Caplan, B. E. Deal, and R. R. Razouk, *J. Appl. Phys.* **52**, 879 (1981).
 - ²¹ E. H. Poindexter, G. J. Gerardi, M.-E. Rueckel, P. J. Caplan, N. M. Johnson, and D. K. Biegelsen, *J. Appl. Phys.* **56**, 2844 (1984).
 - ²² A. Stesmans, *Zeitschrift für Physikalische Chemie Neue Folge* **151**, 191 (1987).
 - ²³ Y. Y. Kim and P. M. Lenahan, *J. Appl. Phys.* **64**, 3551 (1988).
 - ²⁴ A. Stesmans and K. Vanheusden, *Phys. Rev. B* **44**, 11353 (1991).
 - ²⁵ P. M. Lenahan and J. F. Conley, *J. Vac. Sci. Technol. B* **16**, 2134 (1998).
 - ²⁶ R. Müller, P. Kanschä, S. von Aichberger, K. Lips, and W. Fuhs, *J. Non-Cryst. Sol.* **266–269**, 1124 (2000).
 - ²⁷ D. R. McCamey, H. Huebl, M. S. Brandt, W. D. Hutchison, J. C. McCallum, R. G. Clark, and A. R. Hamilton, *Applied Physics Letters* **89**, 182115 (2006).
 - ²⁸ D. R. McCamey, G. W. Morley, H. A. Seipel, L. C. Brunel, J. van Tol, and C. Boehme, *Phys. Rev. B* **78**, 045303 (2008).
 - ²⁹ F. Friedrich, C. Boehme, and K. Lips, *J. Appl. Phys.* **97**, 056101 (2005).
 - ³⁰ C. Boehme, F. Friedrich, T. Ehara, and K. Lips, *Thin Solid Films* **487**, 132 (2005).
 - ³¹ C. Boehme and K. Lips, *Physica B* **376–377**, 930 (2006).
 - ³² K. L. Brower, *Appl. Phys. Lett.* **43**, 1111 (1983).
 - ³³ M. Cook and C. T. White, *Phys. Rev. B* **38**, 9674 (1988).
 - ³⁴ Y. Nishi, T. Tanaka, and A. Ohwada, *Jpn. J. Appl. Phys.* **11**, 85 (1972).
 - ³⁵ B. Koiller, X. Hu, and S. Das Sarma, *Phys. Rev. Lett.* **66**, 027903 (2002).
 - ³⁶ C. J. Wellard and L. C. L. Hollenberg, *Phys. Rev. B* **72**, 085202 (2005).
 - ³⁷ G. W. Morley, D. R. McCamey, H. Seipel, L. C. Brunel, J. van Tol, and C. Boehme, *Phys. Rev. Lett.* **101**, 207602 (2008).
 - ³⁸ G. Feher, *Journal of Physics and Chemistry of Solids* **8**, 486 (1959).
 - ³⁹ D. R. McCamey, H. A. Seipel, S.-Y. Paik, M. J. Walter, N. J. Borys, J. M. Lupton, and C. Boehme, *Nature Materials* **7**, 723 (2008).
 - ⁴⁰ C. Boehme and K. Lips, *Phys. Rev. B* **68**, 245105 (2003).
 - ⁴¹ B. I. Shklovskii, H. Fritsche, and S. D. Baranovskii, *Phys. Rev. Lett.* **62**, 2989 (1989).
 - ⁴² A. Gliesche, C. Michel, V. Rajevac, K. Lips, S. D. Baranovskii, F. Gebhard, and C. Boehme, *Phys. Rev. B* **77**, 245206 (pages 7) (2008).
 - ⁴³ Feher, G., Gere, and E. A., *Phys. Rev.* **114**, 1245 (1959).
 - ⁴⁴ D. Kaplan, I. Solomon, and N. F. Mott, *J. Phys. (Paris) – Lettres* **39**, L51 (1978).
 - ⁴⁵ A. Schweiger and G. Jeschke, *Principles of pulse electron paramagnetic resonance* (Oxford University press, Oxford, 2001).
 - ⁴⁶ R. N. Ghosh and R. H. Silsbee, *Phys. Rev. B* **46**, 12508 (1992).
 - ⁴⁷ C. C. Lo, J. Bokor, T. Schenkel, A. M. Tyryshkin, and S. A. Lyon, *Appl. Phys. Lett.* **91**, 242106 (2007).
 - ⁴⁸ L. H. Willems van Beveren, H. Huebl, D. R. McCamey, T. Duty, A. J. Ferguson, R. G. Clark, and M. S. Brandt, *Appl. Phys. Lett.* **93**, 072102 (2008).
 - ⁴⁹ M. Sarovar, K. C. Young, T. Schenkel, and K. B. Whaley, *Physical Review B* **78**, 245302 (2008).
 - ⁵⁰ R. de Sousa, C. C. Lo, and J. Bokor, eprint arXiv:0806.4638v1 (2008).